AAS 24-428

ADVANCED AUTONOMOUS NUMERICAL PREDICTOR-CORRECTOR GUIDANCE WITH FINAL ALTITUDE AND VELOCITY CONSTRAINTS

Youngro Lee*, Dae Young Lee†, and Bong Wie‡

The numerical predictor-corrector guidance with a bank angle parameterization has been employed in various entry examples where only a final range constraint is present. However, a future human Mars landing mission requires an accurate final location and a precise final altitude and velocity at the end of the entry trajectory. This paper proposes to use a quadratic bank parameterization to generate an entry trajectory that satisfies the multi-constraints. A solution space analysis confirms the numerical feasibility of the proposed guidance algorithm. Monte Carlo simulation results demonstrate the potential applicability of the proposed method for the future Human Mars landing mission.

INTRODUCTION

A numerical predictor-corrector guidance (NPCG) with a linear bank angle parameterization has been widely utilized in various atmospheric entry guidance applications.[1–4] Since the NPCG algorithm directly employs nonlinear dynamics to achieve accurate prediction of the entry vehicle's motion, it can provide a high targeting accuracy in the presence of dispersions and randomness. Because of its capability and applicability, it is now being considered a candidate to be used for a future human Mars landing mission.[5,6]

The computational effectiveness of the NPCG algorithm is attributed to the bank angle parameterization. Assuming a bank angle solution in a specific shape transforms the nonlinear entry guidance problem into a parameter-seeking problem, allowing for efficient onboard computation. Among various kinds of shapes, the linear bank angle has been most frequently adopted in various entry applications. This paper refers to it as the linear bank angle parameterization-based numerical predictor-corrector guidance (LNPCG).

Our previous study[7] revealed that the LNPCG can encounter the challenge of generating an entry trajectory that satisfies the final entry condition for a future human Mars entry, descent, and landing (EDL) mission. Excessive energy dissipation during the early entry phase caused by the linear bank angle leads to the failure to satisfy the final entry state requirement. To tackle that issue, we proposed a novel bank angle parameterization utilizing a logistic function, and a guideline for determining a guidance activation point. The proposed method successfully mitigated the energy dissipation rate during the early entry phase such that higher final altitudes can be achieved compared to the

*Ph.D. Candidate, Department of Aerospace Engineering, Iowa State University, 537 Bissell Rd, Ames, IA, 50011.
†Assistant Professor, Department of Aerospace Engineering, Iowa State University, 537 Bissell Rd, Ames, IA, 50011.
‡Professor, Department of Aerospace Engineering, Iowa State University, 537 Bissell Rd, Ames, IA, 50011.

LNPCG. Note that the proposed method was developed based on the baseline NPCG algorithm, which is a targeting guidance algorithm.

The baseline NPCG algorithm performs dynamic propagation, from a predetermined initial to final energy states, to compute a guidance parameter σ_0 that satisfies the final range constraint.[8] However, this approach causes an issue in satisfying the final conditions of the entry phase. This is due to the fact that because energy is a function of altitude and velocity, multiple combinations of altitude and velocity can result in the same energy value. Therefore, without having an additional algorithm, there's no guarantee that a desired final altitude and velocity set will be achieved at the end of the entry trajectory. The detailed analysis on this is in our previous study.[7]

Various bank angle parameterizations have been proposed to improve the limited capability of the LNPCG. The research in Reference 9 proposed an exponential decaying bank angle parameterization to avoid control saturation during the entry flight. They found that exponential decay maintains greater control authority in the late entry phase compared to assuming constant or linear bank angles. The authors in Reference 10 realized that the linear bank angle parameterization could lead to a final altitude mismatch. To satisfy the final altitude constraint, they proposed a piecewise linear bank angle profile with fixed initial and final bank angles, while the NPC technique determines the middle point bank angle. In Reference 4, a quadratic bank angle parameterization was proposed to generate entry trajectories that satisfy the range and time constraints for multi-hypersonic vehicles. None of these approaches has been applied to the Human Mars mission, which requires an accurate final location and a precise final altitude and velocity at the end of the entry trajectory.

This study proposes an entry guidance algorithm that can concurrently constrain the final range and the final entry state by utilizing a quadratic bank angle parameterization. A solution space analysis of the proposed guidance method verifies that a multi-dimensional problem has a unique solution and numerical feasibility. Furthermore, the Monte Carlo method is used to demonstrate that the proposed guidance method outperforms the LNPCG. The proposed guidance scheme is called advanced autonomous numerical predictor-corrector guidance (A^2NPCG).

The contributions of this paper can be summarized as follows. Firstly, an entry guidance method is developed based on the existing quadratic bank parameterization that can concurrently constrain the final range and the entry state constraints. Secondly, the numerical feasibility of the proposed guidance method is proved by a solution space analysis. Lastly, it is revealed that the proposed entry guidance can outperform the LNPCG in satisfying the final entry state requirements.

The remainder of the paper is structured as follows: First, the atmospheric entry guidance problem of the future human Mars landing mission is outlined. The following section provides an overview of the autonomous numerical predictor-corrector guidance (ANPCG) proposed in our previous study.[7] In the next section, the proposed entry guidance is developed with a detailed analysis. The last section concludes the paper.

PROBLEM FORMULATION

Equations of Motion

The three degree-of-freedom (DOF) equations of motion of an entry vehicle with respect to the spherical Mars-centered-rotating (MCR) and the north-east-down (NED) reference frames (see Fig-

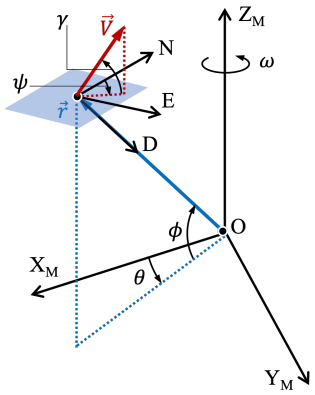

Figure 1. The Mars-centered-rotating (MCR) and the north-east-down (NED) frames.[11]

ure 1) are given by

$$\dot{r} = V \sin\gamma \tag{1a}$$

$$\dot{\theta} = \frac{V \cos\gamma \sin\psi}{r \cos\phi} \tag{1b}$$

$$\dot{\phi} = \frac{V \cos\gamma \cos\psi}{r} \tag{1c}$$

$$\dot{V} = -D - g \sin\gamma + \omega^2 r \cos\phi \left(\sin\gamma \cos\phi - \cos\gamma \sin\phi \cos\psi\right) \tag{1d}$$

$$\dot{\gamma} = \frac{L \cos\sigma}{V} + \left(\frac{V}{r} - \frac{g}{V}\right) \cos\gamma \tag{1e}$$
$$+ 2\omega \cos\phi \sin\psi + \frac{\omega^2 r}{V} \cos\phi \left(\cos\gamma \cos\phi + \sin\gamma \sin\phi \cos\psi\right)$$

$$\dot{\psi} = \frac{L \sin\sigma}{V \cos\gamma} + \frac{V}{r} \cos\gamma \sin\psi \tan\phi \tag{1f}$$
$$+ 2\omega \left(\sin\phi - \tan\gamma \cos\phi \cos\psi\right) + \frac{\omega^2 r}{V \cos\gamma} \sin\phi \cos\phi \sin\psi$$

where r is the radial distance from the center of Mars; θ is the longitude measured from the prime meridian; ϕ is the latitude measured from the equator; V is the relative ground velocity of the entry vehicle to the rotating Mars surface; γ is the relative flight-path angle measured from the local horizontal plane; ψ is the relative heading (or azimuth) angle measured from the north in a clockwise direction; ω is the Mars spin rate; and σ is the bank angle defined as positive to right turn.

The gravitational, lift, and drag accelerations, which are denoted as g, L, and D, are respectively described by

$$g = \frac{\mu}{r^2} \tag{2a}$$

$$L = \left(\frac{1}{2}\rho V^2\right) \frac{C_L S}{m} \tag{2b}$$

$$D = \left(\frac{1}{2}\rho V^2\right) \frac{C_D S}{m} \tag{2c}$$

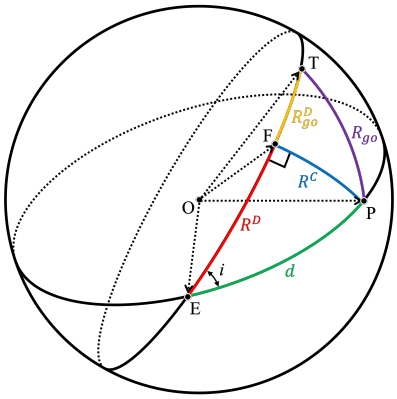

Figure 2. Spherical trigonometry applied to the planetary entry problem.[11]

where μ is the Mars gravitational parameter, C_L and C_D are the lift and drag coefficients, and S and m are the cross-sectional reference area and mass of an entry vehicle, respectively. These five parameters are assumed to be constant. The ballistic coefficient of the entry vehicle is defined as

$$\beta = \frac{m}{C_D S} \tag{3}$$

This study assumes that the entry vehicle maintains trim condition so the lift-over-drag ratio L/D remains constant.

In addition to the six variables in Eq. (1), the range denoted as s is often adopted as a state variable for range control guidance methods.[1,12,13] s indicates the flight distance traveled from the entry interface to the current location such that

$$\dot{s} = V \cos\gamma \tag{4}$$

Entry Path Constraints

A guidance system should monitor and handle the entry path constraints such as g-load A, dynamic pressure q, and aerodynamic heating rate $\dot{Q}$, which are defined as

$$A = \sqrt{L^2 + D^2} \leq A_{max} \tag{5a}$$

$$q = \frac{1}{2}\rho V^2 \leq q_{max} \tag{5b}$$

$$\dot{Q} = k\rho^N V^M \leq \dot{Q}_{max} \tag{5c}$$

where the subscript "max" indicates the allowable limits for each quantity. G-load and dynamic pressure are associated with the safety of payloads, entry vehicle design, and astronauts. The thermal protection system of entry vehicles determines the value of $\dot{Q}_{max}$, and the parameters of the heat flux model are assumed as $N = 0.5$, $M = 3.15$, and $k = 5.3697 \times 10^{-5}$.[14] Note that the proposed guidance method in this study does not include a path constraint handling method. Instead, we discuss how high margins in the path constraints remain for the entry trajectories designed by the proposed method.

Distance Measures

Figure 2 shows a unit sphere in which the initial entry, current, and target locations of the entry vehicle are denoted as $E(\theta_0, \phi_0)$, $P(\theta, \phi)$, and $T(\theta_t, \phi_t)$, respectively. The crossrange R^C and downrange R^D in units of radians can be calculated by using the relationships between arcs and angles of a spherical polygon defined by intersecting great circles as follows:

$$R^C = \sin^{-1}(\sin i \ \sin d) \tag{6a}$$

$$R^D = \cos^{-1}\left(\frac{\cos d}{\cos R^C}\right) \tag{6b}$$

where the great circle distance d, in units of radians, between two points E and P is computed as

$$d = \cos^{-1}(\sin\phi_0 \sin\phi + \cos\phi_0 \cos\phi \cos(\theta - \theta_0)) \tag{7}$$

The angle i, represented with a double-headed arrow in Figure 2, is measured using a set of normal vectors as

$$i = \cos^{-1}(\hat{n}_{OEP} \cdot \hat{n}_{OET}) \tag{8}$$

where the normal vectors are defined as

$$\hat{n}_{OEP} = \frac{\hat{r}_{OE} \times \hat{r}_{OP}}{\|\hat{r}_{OE} \times \hat{r}_{OP}\|} \tag{9a}$$

$$\hat{n}_{OET} = \frac{\hat{r}_{OE} \times \hat{r}_{OT}}{\|\hat{r}_{OE} \times \hat{r}_{OT}\|} \tag{9b}$$

The crossrange R^C can have either positive or negative value depending on the entry vehicle's location with respect to the great-circle line that connects the initial and target locations ($\widehat{ET}$ in Figure 2). Equivalently, the sign of crossrange can be determined by the relationship between a set of normal vectors in the unit sphere. If an entry vehicle is flying on the right side of $\widehat{ET}$, the following holds:

$$\frac{\hat{n}_{OEP} \times \hat{n}_{OET}}{\|\hat{n}_{OEP} \times \hat{n}_{OET}\|} \cdot \hat{r}_{OE} > 0 \tag{10}$$

In the case of the entry vehicle flying left side of $\widehat{ET}$, the sign of Eq. (10) becomes negative.

The downrange-to-go, denoted as R^D_{go}, which corresponds to the arc $\widehat{FT}$, expresses the missed distance in the longitudinal direction. One can noticed that R_{go} is a combination of R^D_{go} and R^C, as shown in Figure 2.

Human Mars Atmospheric Entry Mission

The atmospheric entry phase of the future human Mars mission is currently under development led by NASA so some of their specific information has not been fully determined yet. Table 1 provides a set of the numerical data of a reference mission model studied in this paper. Note that the entry interfaces and target locations are given in the MCR and NED frames. References 5, 14–18 are mainly used to formulate the entry example addressed in this paper.

The Martian air density model in Reference 22 is used here, which is given by

$$\rho(h) = \rho_0 \exp(-0.000105h) \tag{11}$$

Table 1. Human Mars atmospheric entry mission

	Symbols	Values
Entry Interface[15]	h_0	125 km
	θ_0	-176.40167 deg
	ϕ_0	-21.3 deg
	V_0	4700 m/s
	γ_0	-10 deg
	ψ_0	-2.8758 deg
Final Condition[15]	θ_t	-175.8 deg
	ϕ_t	0.276 deg
	V_t	450 m/s
	h_t	2480 m
Targeting Accuracy Requirement[19]	$R_{go}(t_f)$	$\leq$ 5 km
Initial Range-to-go	$R_{go}(t_0)$	1279.4 km
Entry Vehicle Aerodynamic Property[20]	L/D	0.54
	β	379 kg/m^2
Path Constraints Requirements[21]	A	$\leq$ 4g
	q	$\leq$ 13 kPa
	$\dot{Q}$	$\leq$ 500 kW/m^2

where h is the altitude in units of kilometers from the Martian surface, and the reference air density ρ_0 is a function of temperature T with two constants $\alpha_1 = 559.35$ and $\alpha_2 = 188.95$ as

$$\rho_0 = \frac{\alpha_1}{\alpha_2 T} \tag{12}$$

where

$$T = 1.4 \times 10^{-13} h^3 - 8.85 \times 10^{-9} h^2 - 1.245 \times 10^{-3} h + 205.36 \tag{13}$$

The entry vehicle is called the Cobra mid lift-to-drag ratio rigid vehicle (CobraMRV), which utilizes an aero-propulsive control strategy, including aero-surfaces and Reaction Control System (RCS) thrusters. For simplicity, the simulation framework in this paper does not consider the magnitude and rate constraints on the bank angle control, and guidance commands are applied to the dynamical model without any attitude control latency. The development of more realistic scenarios will be addressed in future work. The feasibility analysis on the CobraMRV's flight control system can be found in References 5, 16.

Some parameters used in the simulations are: the Mars gravitational parameter μ is 42828 km^3/s^2, the Mars radius r_m is 3397 km, and the Mars spin rate ω is 7.088 $\times$ 10^{-5} rad/s. The simulations are conducted using MATLAB® R2022a on a MacBook Pro with 2.6 GHz 6-core Intel Core i7 and 16 GB of DDR4 RAM. MATLAB's *ODE45* is used as a numerical integrator.

AUTONOMOUS NUMERICAL PREDICTOR-CORRECTOR GUIDANCE

This section briefly describes the autonomous numerical predictor-corrector guidance (ANPCG) algorithm and displays a reference design for the entry trajectory of the human Mars landing mission.

Algorithm Description

The ANPCG was developed based on the baseline NPCG algorithm in that it solves a final range constraint problem using a parameterized bank profile. The NPC technique seeks a guidance parameter σ_0 at every guidance cycle and a design input K that adjusts guidance performance. In contrast to the existing linear bank angle parameterization approach, the ANPCG can automatically alter the final bank angle magnitude according to the σ_0 value. The logistic function-based bank angle parameterization is given by

$$\sigma_{cmd}(e) = \frac{2\sigma_0}{1 + \exp\left[K(e - e_0)/(e_f - e_0)\right]} \tag{14}$$

where the parameter K represents the decay rate, adjusting how quickly the bank angle reduces, e_0 is the current energy state, and e_f is the given final energy state. Note that σ_{cmd} at e_0 is σ_0 regardless of K, whereas σ_{cmd} at e_f is affected by K. A larger value of K tends to cause a higher final altitude and peaks of path constraints of the entry trajectory. The range of K value that leads to a proper guidance performance was found around one.

The baseline NPCG algorithm consists of two steps: prediction and correction. At the prediction step, a trajectory propagation from e_0 to e_f is conducted using Eq. (1). Then, the correction step is carried out iteratively until the parameterized bank angle profile results in a trajectory that satisfies the following final range constraint:

$$z(\sigma_0) = s(e_f) - s_f = 0 \tag{15}$$

where $s(e_f)$ is the actual distance traveled at e_f and $s_f = s_{go} = R_{go}$ is the range-to-go to the target site at the current guidance cycle. Note that the computational process employs normalized state variables, where the length is normalized by the Mars radius, the velocity is normalized by the orbital velocity at the Mars radius, and the time is scaled accordingly.

The numerical propagations and the bank angle parameterization inside the guidance algorithm utilize a dimensionless energy-like variable e, which is defined as

$$e = \frac{\mu}{r} - \frac{V^2}{2} \equiv -\mathcal{E} \tag{16}$$

where $\mathcal{E}$ is the conventional specific energy. Taking the derivative of e with respect to time and using dr/dt and dV/dt from Eq. (1) results in the following relationship:

$$\dot{e} = DV \tag{17}$$

which indicates that e monotonically increases. Energy-based propagation eliminates the need for flight time information but necessitates the use of final values for altitude and velocity to define the endpoint.

The Newton-Raphson method is employed to find σ_0 satisfying Eq. (15). For a given initial guess $\sigma_0^{(0)}$, the k^{th} update for $\sigma_0^{(k)}$ is performed as

$$\sigma_0^{(k+1)} = \sigma_0^{(k)} - \frac{z(\sigma_0^{(k)})}{\partial z(\sigma_0^{(k)})/\partial \sigma_0} \tag{18}$$

where the partial derivative of Eq. (15) with respect to σ_0 is computed by the centered finite difference approximation with a given small increment $\Delta\sigma$ as

$$\frac{\partial z(\sigma_0^{(k)})}{\partial \sigma_0} \approx \frac{z(\sigma_0^{(k)} + \Delta\sigma) - z(\sigma_0^{(k)} - \Delta\sigma)}{2\Delta\sigma} \tag{19}$$

The corrective update continues until the absolute value of Eq. (15) becomes less than a small positive number ϵ. In this study, ϵ and the initial guess for σ_0 are set to one hundred meters and 100 degrees.

Predictive Lateral Guidance

Since the baseline NPCG algorithm is intended to control the longitudinal motion of the entry vehicle, a lateral guidance method is necessary to achieve high-precision landing accuracy. This study utilizes the predictive lateral guidance method proposed in Reference 23. The method assumes that the computed bank angle from the NPCG algorithm is available for final crossrange computations. The two final crossrange values of the entry trajectory for the converged bank command, which is set to be either positive or negative throughout the entire trajectory, are then determined. If the ratio between two crossrange values exceeds a certain threshold, then a bank reversal occurs. That ratio is set to seven for all simulation results presented in this paper. Note that the initial bank angle direction is determined as the opposite direction to the heading angle error.

A Reference Design for the CobraMRV's Entry Trajectory

Figure 3 shows the entry trajectory generated by the ANPCG algorithm. The entry trajectory generated by the ANPCG satisfies the final state requirement (2.48 km altitude and 450 m/s velocity) and achieves less than 100 meters of final range error. Note that the decay rate K and the guidance system activation timing $t_g a$ are set to be 1.28 and 175 sec for a satisfying guidance performance. If random dispersions on the entry interface or aerodynamic models are present, the final state of the ANPCG's entry trajectory is likely to deviate from the final state requirement. Even without a path constraints handling algorithm, there is about a 10% margin in the g-load and dynamic pressure constraints and about a 30% margin in the aerodynamic heating rate.

ADVANCED AUTONOMOUS NUMERICAL PREDICTOR-CORRECTOR GUIDANCE

Although the ANPCG can generate the entry trajectory that satisfies the final state requirements, it requires precise adjusting the decay rate k such that the entry trajectory ends at the desired altitude and velocity. Since the baseline NPCG algorithm constructs the bank profile in the energy domain from e_0 to e_f, constraining either one of the final altitude and the final velocity means constraining the other. If the bank angle parameterization can take one more guidance parameter, it can handle an additional constraint, which is the basic idea of the A^2NPCG algorithm.

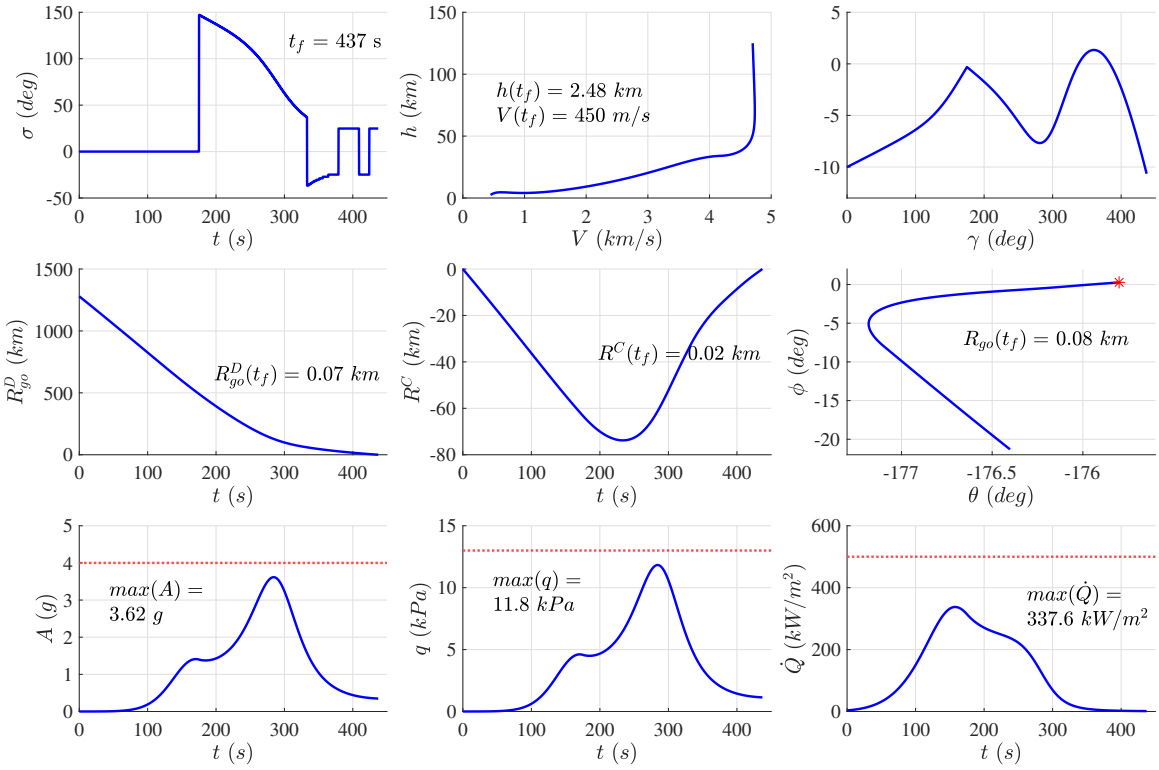

Figure 3. The entry trajectory generated by the ANPCG.

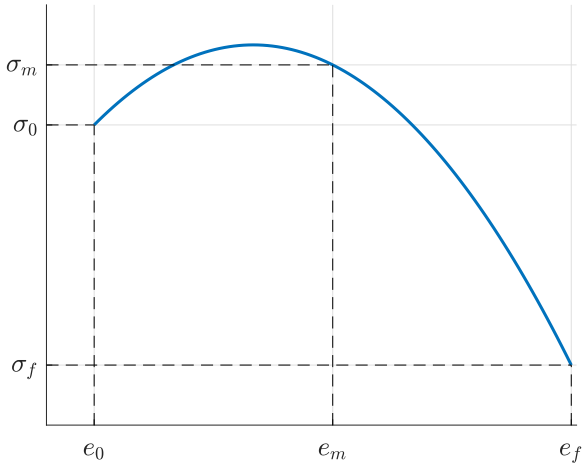

Figure 4. The quadratic bank angle profile that is parameterized by σ_0, σ_m, and σ_f.

Algorithm Description

The quadratic bank angle parameterization was proposed in Reference 4 to generate the entry trajectory that simultaneously meets the final range and flight time constraints. Maintaining the quadratic bank angle parameterization but changing the formula can fulfill the entry trajectory design of the CobraMRV mission in which precise velocity and altitude conditions at the end of the

entry trajectory are demanded. The quadratic bank angle parameterization is given by

$$\begin{aligned}\sigma_{cmd}(e) = & \frac{2\left(\sigma_0 - 2\sigma_m + \sigma_f\right)}{\left(e_0 - e_f\right)} e^2 \\ & - \frac{\sigma_0 e_0 + 3\sigma_0 e_f - 4\sigma_m e_0 - 4\sigma_m e_f + \sigma_f e_0 + \sigma_f e_f}{\left(e_0 - e_f\right)^2} e \\ & + \frac{\sigma_0 e_0 e_f + \sigma_0 e_f^2 - \sigma_m e_0 e_f + \sigma_f e_0^2 + \sigma_f e_0 e_f}{\left(e_0 - e_f\right)^2}\end{aligned} \tag{20}$$

where σ_0 is the bank angle magnitude at the current energy state e_0, σ_m is the bank angle magnitude at midpoint energy $e_m = \left(e_0 + e_f\right)/2$, and σ_f is a positive constant. Figure 4 shows the quadratic bank profile shaped by σ_0, σ_m, and σ_f. Since the quadratic bank parameterization has two guidance parameters ($\boldsymbol{u} = [\sigma_0 \ \sigma_m]^T$), it can have higher flexibility than Eq. (14). Along with the final range constraint, the final altitude constraint is included in the A^{2}NPCG algorithm:

$$\boldsymbol{Z}\left(\boldsymbol{u}\right) = \begin{bmatrix} z_1 \\ z_2 \end{bmatrix} = \begin{bmatrix} s(e_f) - s_f \\ h(e_f) - h_f \end{bmatrix} = 0 \tag{21}$$

The Newton-Raphson method is also employed to find $\boldsymbol{u}$ satisfying Eq. (21). The Jacobian of Eq. (21) with respect to $\boldsymbol{u}$ is required to update a solution, and it is given as

$$\boldsymbol{J} = \begin{bmatrix} \frac{\partial z_1}{\partial \sigma_0} & \frac{\partial z_1}{\partial \sigma_m} \\ \frac{\partial z_2}{\partial \sigma_0} & \frac{\partial z_2}{\partial \sigma_m} \end{bmatrix} \tag{22}$$

The partial derivatives in Eq. (22) are computed in the same technique as Eq.(19). For a given initial guess $\boldsymbol{u}^{(0)}$, the k^{th} update for $\boldsymbol{u}^{(k)}$ is performed as

$$\boldsymbol{u}^{(k+1)} = \boldsymbol{u}^{(k)} - \boldsymbol{J}^{-1}\boldsymbol{Z}(\boldsymbol{u}^{(k)}) \tag{23}$$

where the computation of solution update is conducted by MATLAB's *mldivide*. The corrective update continues until the sum of absolute values of z_1 and z_2 in Eq. (21) becomes less than a small positive number ϵ, which is set to ten meters. The initial guess is given as $\boldsymbol{u}^{(0)} = [90\ deg\ 120\ deg]^T$. Solution space analysis regarding the initial guess is provided in this section later.

A Reference Design for the CobraMRV's Entry Trajectory

Figure 5 shows the entry trajectory generated by the A^{2}NPCG algorithm. σ_f and t_ga are set as 20 deg and 170 sec, respectively. Solution space analysis regarding the variation of σ_f and t_ga is discussed in the following subsection. The final state of the entry trajectory accurately satisfies the mission requirements. The entry trajectories of the ANPCG and the A^{2}NPCG show similarities in many aspects, such as path constraints peak levels. However, the bank angle profile at the early phase of the A^{2}NPCG tends to have a lower magnitude than that of the ANPCG.

Figure 6 presents the bank command profiles plotted every 10^{th} guidance cycle in the energy domain for the entry trajectory shown in Figure 5. At each guidance, the quadratic bank angle parameterized by σ_0, σ_m, and σ_f is sought by the guidance algorithm such that it satisfies the final range and the entry state constraints. It can be observed that the bank profiles maintain a similar shape throughout the trajectory.

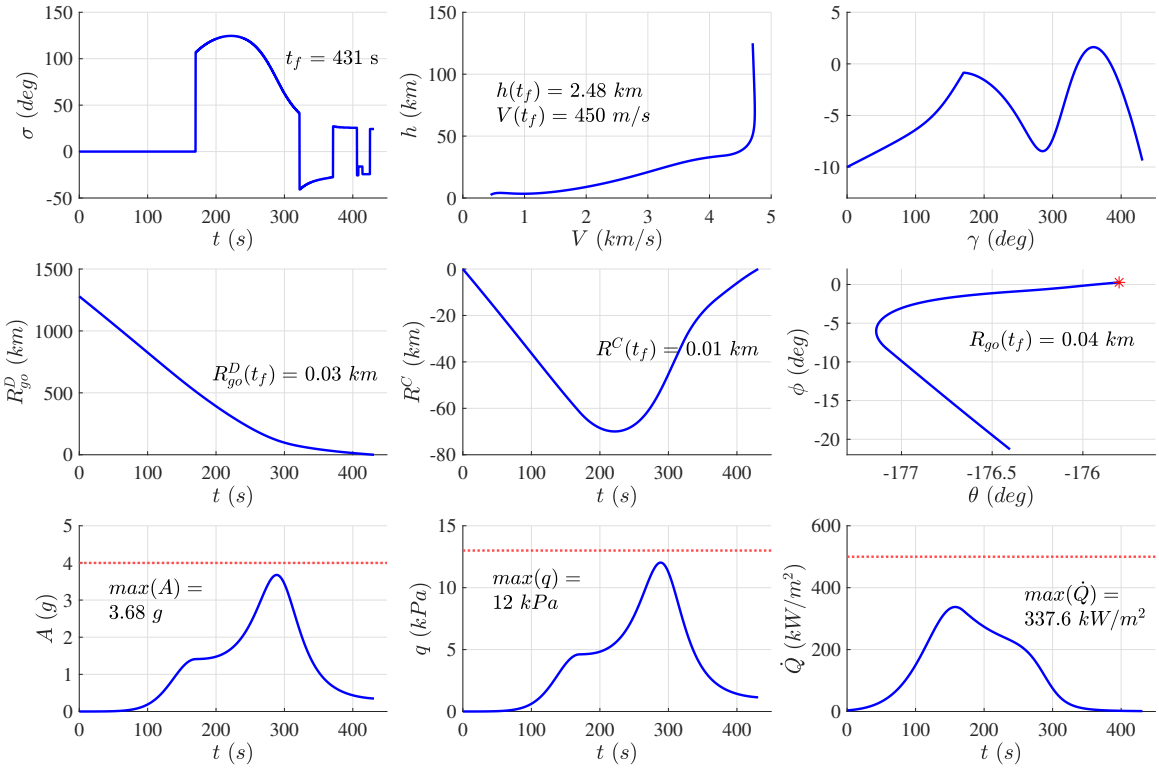

Figure 5. The entry trajectory generated by the A^{2}NPCG.

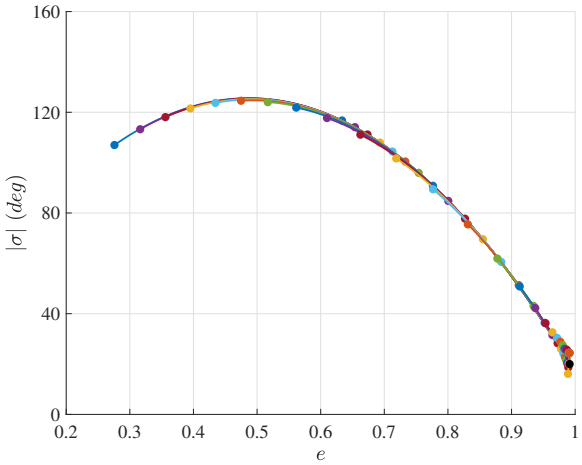

Figure 6. The bank command profiles plotted every 10^{th} guidance cycle in the energy domain.

Solution Space Analysis

Since the proposed guidance algorithm has two guidance parameters, σ_0 and σ_m, to find, the solution-seeking process is likely more intricate than the single guidance parameter approaches, such as the LNPCG and the ANPCG. Therefore, a solution space analysis in the σ_0–σ_m domain is conducted to check the feasibility of the given entry problem comprehensively.

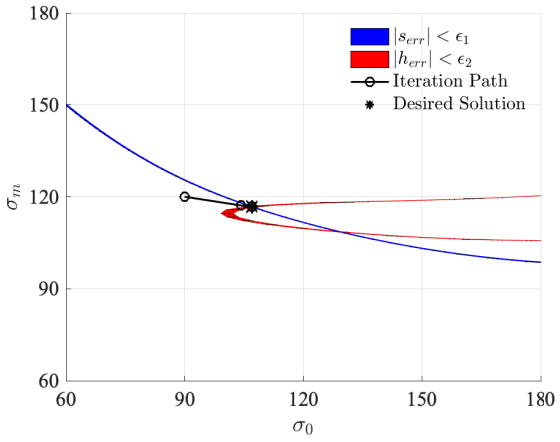

Figure 7. The solution space of the given entry problem when σ_f = 20 deg and $t_g a$ = 170 sec. A solution is found after three steps iterations.

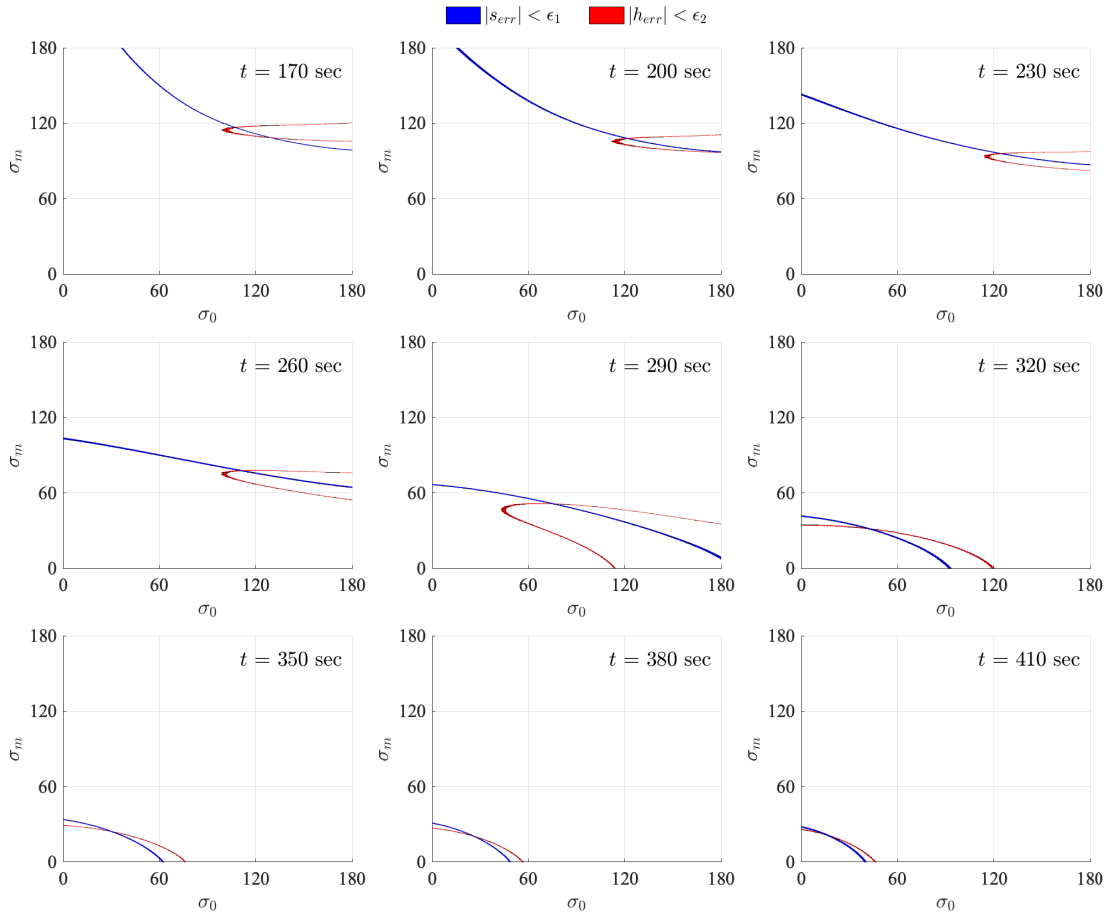

Figure 8. The chronological evolution of the solution space along the entry trajectory when σ_f = 20 deg and $t_g a$ = 170 sec.

Figure 7 displays the solution space of the given entry problem when σ_f = 20 deg and $t_g a$ = 170 sec. The blue and red lines represent the paths where each constraint is satisfied. Since the proposed guidance method concurrently addresses the final range and altitude constraints, a solution that satisfies both constraints needs to be located. It can be noticed that where the red and blue lines intersect is where a solution exists. Out of the two local solutions, only the upper one can produce a feasible entry trajectory until the end, which means that the given entry problem has a unique solution at that guidance cycle. If the initial guess is given as $\boldsymbol{u}^{(0)} = [90\ deg\ 120\ deg]^T$, it takes three steps to converge to the desired solution.

Figure 8 illustrates the chronological evolution of the solution space along the entry trajectory. The top left subfigure is the same as Figure 7 at the moment of guidance law activated. It is evident that one of the local solutions seen in Figure 4 only lasts until 200 seconds, while the other one remains in existence until the end. Therefore, we can conclude that a unique solution to the given problem exists. As the entry vehicle approaches the ground, the magnitudes of σ_0 and σ_m decrease, as seen from Figure 6.

Table 2. Dispersion levels on the entry interface and models.

Parameters	Three-Standard Deviation Distributions[21]
r	100 m
θ	0.25 deg
ϕ	0.25 deg
V	3.3 m/s
γ	0.1 deg
ψ	0.17 deg
m	200 kg
ρ	5%

Monte Carlo Simulation

The Monte Carlo method is adopted to examine the effect of entry interface dispersion and modeling errors on the guidance performance. The entry interface is randomly sampled from a Gaussian distribution with three-standard deviations (SD), and they are given in Table 2. A 1000-run Monte Carlo simulation is conducted for each guidance method.

Figure 9 presents the results of Monte Carlo simulations comparing the performance of the ANPCG and A^{2}NPCG, and Table 3 summarizes the statistical data. Both methods demonstrate their robustness over randomness in satisfying the targeting accuracy requirement (5 km). As we intended in the guidance algorithm, the A^{2}NPCG has the entry trajectories to terminate around the desired final state in a more concentrated form than the ANPCG. The SDs of the final altitude and velocity of the A^{2}NPCG are about three times lower than that of the ANPCG. Although the average final targeting error of the A^{2}NPCG is higher the that of the ANPCG, it is a reasonable sacrifice considering the mission requirement.

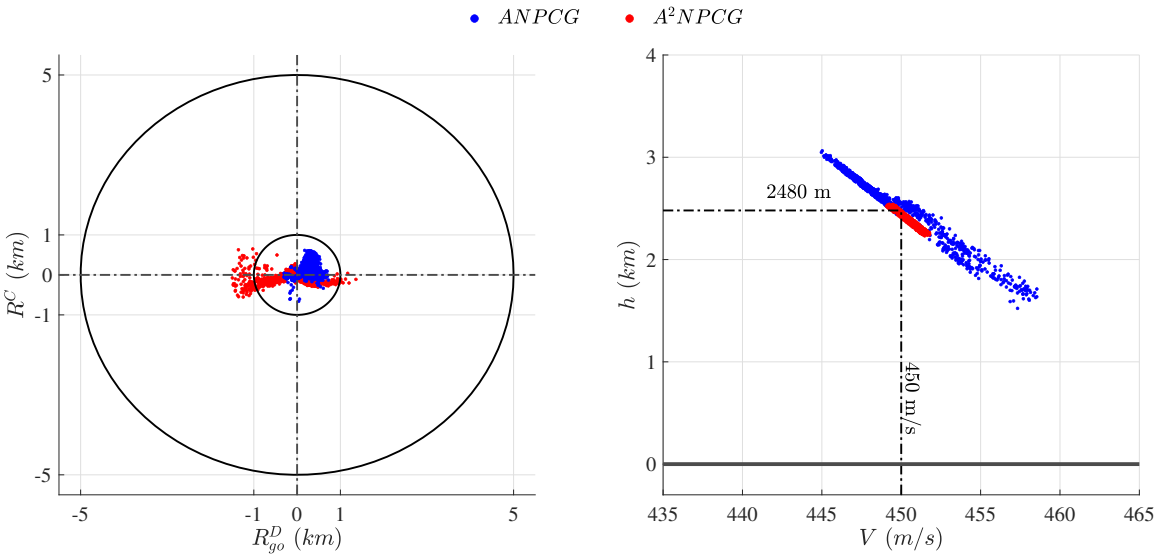

Figure 9. The Monte Carlo simulation results comparing the ANPCG and A^{2}NPCG. Left: the final range dispersions. Right: the final altitude and velocity dispersions.

Table 3. The statistics of the Monte Carlo simulation results: M and SD are mean, median, and standard deviation operators, respectively.

Statistics	ANPCG	A^{2}NPCG	Statistics	ANPCG	A^{2}NPCG
$M[R_{go}(t_f)]$	273 m	446 m	$M[max(A)]$	3.6g	3.7g
$SD[R_{go}(t_f)]$	208 m	374 m	$SD[max(A)]$	0.1g	0.1g
$M[h(t_f)]$	2487 m	2415 m	$M[max(q)]$	11.9 kPa	12.0 kPa
$SD[h(t_f)]$	334 m	96 m	$SD[max(q)]$	0.3 kPa	0.3 kPa
$M[V(t_f)]$	450 m/s	450 m/s	$M[max(\dot{Q})]$	337.5 kW/m^2	337.5 kW/m^2
$SD[V(t_f)]$	3 m/s	1 m/s	$SD[max(\dot{Q})]$	2.9 kW/m^2	3.0 kW/m^2

CONCLUSION

This paper proposed using quadratic bank parameterization to generate the entry trajectory for the future human EDL mission, requiring precise final location, altitude, and velocity. The Monte Carlo simulation demonstrated that the A^{2}NPCG outperforms the lower dimension bank parameterization approach as it can simultaneously satisfy multiple constraints. Furthermore, the solution space analysis revealed that the multi-dimensional problem has a unique solution leading to a feasible entry trajectory. The presented simulation results and analysis indicated that the proposed guidance method could be suitable for future human Mars EDL missions.

REFERENCES

[1] P. Lu, "Entry Guidance: A Unified Method," *Journal of Guidance, Control, and Dynamics*, Vol. 37, No. 3, 2014, pp. 713–728, 10.2514/1.62605.

[2] P. Lu, S. Forbes, and M. Baldwin, "Gliding Guidance of High L/D Hypersonic Vehicles," *AIAA Guidance, Navigation, and Control (GNC) Conference*, 2013, 10.2514/6.2013-4648.

[3] T. Wang, H. Zhang, and G. Tang, "Predictor-corrector entry guidance with waypoint and no-fly zone constraints," *Acta Astronautica*, Vol. 138, 2017, pp. 10–18, https://doi.org/10.1016/j.actaastro.2017.05.009.

[4] Z. Li, B. He, M. Wang, H. Lin, and X. An, "Time-coordination entry guidance for multi-hypersonic vehicles," *Aerospace Science and Technology*, Vol. 89, 2019, pp. 123–135, https://doi.org/10.1016/j.ast.2019.03.056.

[5] B. J. Johnson, C. J. Cerimele, S. Stachowiak, R. R. Sostaric, D. A. Matz, and P. Lu, "Mid-Lift-to-Drag Ratio Rigid Vehicle Control System Design and Simulation for Human Mars Entry," *2018 AIAA Guidance, Navigation, and Control Conference*, 2018, 10.2514/6.2018-0615.

[6] R. A. Lugo, R. Powell, and A. M. Dwyer-Cianciolo, "Overview of a Generalized Numerical Predictor-Corrector Targeting Guidance with Application to Human-Scale Mars Entry, Descent, and Landing," *AIAA Scitech 2020 Forum*, 2020, 10.2514/6.2020-0846.

[7] Y. Lee, D. Y. Lee, and B. Wie, "Autonomous Numerical Predictor-Corrector Guidance for Human Mars Landing Missions," *Aerospace Science and Technology (under review)*.

[8] P. Lu, "Predictor-Corrector Entry Guidance for Low-Lifting Vehicles," *Journal of Guidance, Control, and Dynamics*, Vol. 31, No. 4, 2008, pp. 1067–1075, 10.2514/1.32055.

[9] Z. Liang and S. Zhu, "Constrained predictor-corrector guidance via bank saturation avoidance for low L/D entry vehicles," *Aerospace Science and Technology*, Vol. 109, 2021, p. 106448, https://doi.org/10.1016/j.ast.2020.106448.

[10] W. J. Zhang and B. M. Wang, "Predictor corrector algorithms considering multiple constraints for entry vehicles," *The Aeronautical Journal*, Vol. 126, No. 1305, 2022, p. 1874–1896, 10.1017/aer.2022.19.

[11] Y. Lee, D. Y. Lee, and B. Wie, "A comparative study of entry guidance for Mars robotic and human landing missions," *Acta Astronautica*, Vol. 215, 2024, pp. 178–193, https://doi.org/10.1016/j.actaastro.2023.11.045.

[12] R. Furfaro and D. Wibben, "Mars Atmospheric Entry Guidance via Multiple Sliding Surface Guidance for Reference Trajectory Tracking," *AIAA/AAS Astrodynamics Specialist Conference*, 2012, 10.2514/6.2012-4435.

[13] K. D. Webb and P. Lu, "Entry Guidance by Onboard Trajectory Planning and Tracking," *AIAA Atmospheric Flight Mechanics Conference*, 2016, 10.2514/6.2016-0279.

[14] X. Jiang, S. Li, and R. Furfaro, "Integrated guidance for Mars entry and powered descent using reinforcement learning and pseudospectral method," *Acta Astronautica*, Vol. 163, 2019, pp. 114–129, https://doi.org/10.1016/j.actaastro.2018.12.033.

[15] M. Sagliano, P. Lu, B. Johnson, D. Seelbinder, and S. Theil, "Six-Degrees-of-Freedom Aero-Propulsive Entry Trajectory Optimization," *AIAA SCITECH 2024 Forum*, 2024, 10.2514/6.2024-1171.

[16] J. A. Samareh, "Parametric Trade Study of Mid Lift/Drag Entry Systems for Human Mars Mission," *AIAA Scitech 2020 Forum*, 2020, 10.2514/6.2020-1512.

[17] R. R. Sostaric, C. J. Cerimele, E. A. Robertson, and J. A. Garcia, "A Rigid Mid Lift-to-Drag Ratio Approach to Human Mars Entry, Descent, and Landing," *2017 AIAA Guidance, Navigation, and Control Conference*, 2017, 10.2514/6.2017-1898.

[18] Y. Gong, Y. Guo, G. Ma, and M. Guo, "Mars entry guidance for mid-lift-to-drag ratio vehicle with control constraints," *Aerospace Science and Technology*, Vol. 107, 2020, p. 106361, https://doi.org/10.1016/j.ast.2020.106361.

[19] B. J. Johnson, E. M. Braden, R. R. Sostaric, C. J. Cerimele, and P. Lu, "Entry, descent, and landing performance for a mid-lift-to-drag ratio vehicle at Mars," *2018 American Astronautical Society Guidance and Control Conference*, 2018.

[20] B. J. Johnson, P. Lu, and C. Cerimele, "Mid-Lift-To-Drag Ratio Rigid Vehicle 6-DOF EDL Performance Using Tunable Apollo Powered Guidance," *AAS/AIAA Space Flight Mechanics Meeting*, 2019.

[21] B. J. Johnson, P. Lu, and R. R. Sostaric, "Mid Lift-to-Drag Rigid Vehicle 6-DoF Performance for Human Mars Entry, Descent, and Landing: A Fractional Polynomial Powered Descent Guidance Approach," *AIAA Scitech 2020 Forum*, 2020, 10.2514/6.2020-1513.

[22] S. C. Paschall, *Mars Entry Navigation Performance Analysis Using Monte Carlo Techniques*. PhD thesis, Massachusetts Institute of Technology. Dept. of Aeronautics and Astronautics., 2004.

[23] K. M. Smith, "Predictive lateral logic for numerical entry guidance algorithms," *AAS/AIAA Space Flight Mechanics Meeting*, 2016.